World Journal of Otorhinolaryngology-Head and Neck Surgery (2021) 7, 9—16

Available online at www.sciencedirect.com

ScienceDirect

journal homepage: www.keaipublishing.com/WJOHNS; www.wjent.org

Research Paper

Radiologic anatomy of the round window relevant to cochlear implantation and inner ear drug delivery☆

Peter L. Nguy [a], Sheela Saidha [b], Ann Jay [c], H. Jeffrey Kim [a], Michael Hoa [a,*]

[a] Department of Otolaryngology-Head and Neck Surgery, Georgetown University Medical Center, Washington DC, USA
[b] Department of Otolaryngology, University of Rochester Medical Center, Rochester, NY, USA
[c] Department of Radiology, Georgetown University Medical Center, Washington DC, USA

Received 16 August 2018; received in revised form 3 November 2018; accepted 3 December 2018
Available online 20 June 2020

KEYWORDS
Round window;
Cochlear implantation;
Transtympanic drug delivery;
Computed tomography

Abstract *Objective:* To determine anatomic relationships and variation of the round window membrane to bony surgical landmarks on computed tomography.
Study design: Retrospective imaging review.
Methods: 100 temporal bone images were evaluated. Direct measurements were obtained for membrane position. Vector distances and angulation from umbo and bony annulus were calculated from image viewer software coordinates.
Results: The angle of round window membrane at junction with cochlear basal turn was (42.1 ± 8.6)°. The membrane's position relative to plane of the facial nerve through facial recess was (14.7 ± 5.2)° posterior from a reference line drawn through facial recess to carotid canal. Regarding transtympanic drug delivery, the round window membrane was directed 4.1 mm superiorly from the inferior annulus and 5.4 mm anteriorly from the posterior annulus. The round window membrane on average was angled superiorly from the inferior annulus (77.1 ± 27.9)° and slightly anteriorly from the posterior annulus (19.1 ± 11.1°). The mean distance of round window membrane from umbo was 4 mm and posteriorly rotated 30° clockwise from a perpendicular drawn from umbo to inferior annulus towards posterior annulus.

☆ Presented at the Combined Otolaryngology Spring Meeting, American Otological Society; 2015 April 25—28; Boston, Massachusetts, USA.

* Corresponding author. Department of Otolaryngology-Head and Neck Surgery, Georgetown University School of Medicine, 3800 Reservoir Rd, NW, Washington DC 20007, United States. Fax: 202 444 0555.
E-mail address: michael.hoa@gunet.georgetown.edu (M. Hoa).

Peer review under responsibility of Chinese Medical Association.

Production and Hosting by Elsevier on behalf of KeAi

https://doi.org/10.1016/j.wjorl.2018.12.003

Together, these measurements approximate the round window membrane in the tympanic membrane's posteroinferior quadrant.
Conclusions: These radiologic measurements demonstrate normal variations seen in round window anatomy relative to facial recess approach and bony tympanic annulus, providing a baseline to assess round window insertion for cochlear implantation and outlines anatomic factors affecting transtympanic drug delivery.

Introduction

Round window membrane (RWM) position and orientation can present challenges for successful round window insertion (RWI) in cochlear implantation (CI) as well as effective transtympanic drug delivery (TDD). An awareness of anatomic variation may allow for improved patient counseling, fine tuning of surgical approach, and enable improved drug delivery to the inner ear.[1]

RWI may minimize intracochlear trauma during cochlear implant surgery. Compared to RWI, dense fibrosis or new bony formation was discovered at sites of intracochlear trauma with cochleostomy.[2] Implantations via RWI had more appropriate electrode placement in the scala tympani, corresponding to higher consonant-nucleus-consonant word scores.[3] Although these findings do not conclusively link RWI with better outcomes, it is believed that decreased trauma to intracochlear structures benefits postsurgical hearing. Electrode trajectory should parallel the longitudinal axis of the lower basal turn scala tympani. In the event this position is not maintained, the basilar membrane may be directly damaged or secondarily damaged by rebound from the bony cochlear wall.[4] Unfortunately, RWI is not always possible in patients with unfavorable anatomy and expectations should be managed during surgical planning.

Several prior studies have demonstrated the utility of computed tomography (CT) images in evaluating cochlear implant candidates. In their subset of pediatric patients, Tamplen et al[5] reported that 60% had CT findings prompting a change in surgical plan. Other CT studies have highlighted variability in RW anatomy between pediatric and adult populations, highlighting the importance of imaging in preoperative evaluation.[6–8]

Though CI and TDD are different procedures in the neurotologic repertoire, the RWM remains an integral structure to identify for both. Many inner ear disorders, including Meniere's disease and sudden sensorineural hearing loss, can be treated using systemic drug administration. However, this may not be ideal as the blood-labyrinth barrier limits therapeutics from reaching the inner ear.[9] TDD provides an opportunity for direct treatment while minimizing systemic side effects.[10] Improved understanding of RW anatomy thus may improve therapeutic drug delivery to the inner ear.

This study defines a series of radiologic measurements on CT studies relevant to RW localization from tympanic membrane (TM) landmarks for TDD and for RW visualization through the facial recess (FR) for CI. We use a Cartesian-coordinate system generated by a free-to-download DICOM viewer software, which was shown to be reliable and accurate.[11,12] To our knowledge, only one other study has used a coordinate system for preoperative evaluation. Though these authors obtained consistent measurements, the study was limited by a small sample of temporal bones (TB).[13] The authors of this study hope these measurements will be useful in evaluating potential candidates for CI and TDD by highlighting RW anatomic variation and approximating RWM position and orientation to identify unfavorable anatomy.

Methods

An institutional review board-approved retrospective imaging review of CT studies of the internal auditory canal was performed at our institution from June 2014 through December 2014 to obtain radiologic measurements on TBCT studies. Studies with diagnosed fracture, infection, cholesteatoma, tumors, congenital anomalies and repeat studies of the same patient were excluded. Each ear was treated independently.

Imaging was obtained using Siemens 64-channel multidetector CT with resolution of 330 μm in 0.6 mm collimation, reconstructed in 0.2 mm intervals in axial plane with coronal reformatting. One hundred fourteen CT studies were reviewed. Fourteen were excluded based on above exclusion criteria.

Measurements were obtained using OsiriX Lite DICOM Viewer (http://www.osirix-viewer.com/) at 300% magnification. Specifically for vector measurements, landmarks were designated using xyz-coordinates generated by Osirix 'point' function. Vector length and trajectory were calculated using an online tool (https://www.vcalc.com/wiki/vCalc/Vector+Calculator+%283D%29). Statistical analysis was conducted using JMP Pro 11 for all variables.

Measurements relevant to CI

Angle of RWM relative to cochlear basal turn (BT-Coch) [∠RWBT]

At the level of best visibility of the RWM on axial images, a reference angle is drawn at the junction of RWM and the posterior bony boundary of BT-Coch. To obtain the desired angle, the supplementary angle is obtained by subtracting the reference angle from 180° (Fig. 1). This angle is

relevant to neurotologists who visualize the angulation of the RWM through the FR during cochlear implant surgery.

RWM position and visibility from FR

Analysis was performed in the axial plane. When a single image did not visualize the mastoid segment of the facial nerve (FN), the RWM, and the carotid artery (CA), the CT scan data were reformatted to visualize all landmarks on one slice using the 3D multiplanar reconstruction (MPR) tool available within OsiriX Lite DICOM Viewer. A reference line was drawn from the anterior edge of the facial nerve mastoid segment (AFN) to the carotid canal lateral wall. Two subsequent angles were then measured using this reference line: one to the lateraledge of the RWM and the other to the medial boundary of the RWM. The degrees of freedom (∠DOF) between these two angles represent RWM visibility from the facial nerve (angle b in Fig. 2). The angle obtained using the lateral boundary of RWM defines the degrees of adjustment (∠DOA), reflecting RWM position relative to the FN (angle a in Fig. 2). RWM position relative to the FN, as measured by ∠DOA, is particularly relevant to RWM accessibility through the FR for cochlear implant surgery.

Distance and trajectory from FR to midpoint of RWM (mid-RWM)

Axial images were examined at level of the exposed RWM and bony overhang of the RW niche (RWN). Points were marked corresponding to the AFN, RWN, and mid-RWM. A reference line was drawn from AFN to RWN. The line connecting AFN to mid-RWM represented the vector of interest, giving both values of length and angle displaced from the AFN-RWN reference line (Fig. 3). A schematic flow diagram is available online for readers to view as AFN, RWN, and mid-RWM are marked in OsiriX with generation of xyz-coordinates (Supplement 1).

Measurements relevant to TDD

Distance and trajectory from bony tympanic annulus (TA) to mid-RWM

Both axial and coronal images were examined. Anatomical representation of TA varied depending on plane: axial slices depicted posterior TA and coronal images depicted inferior

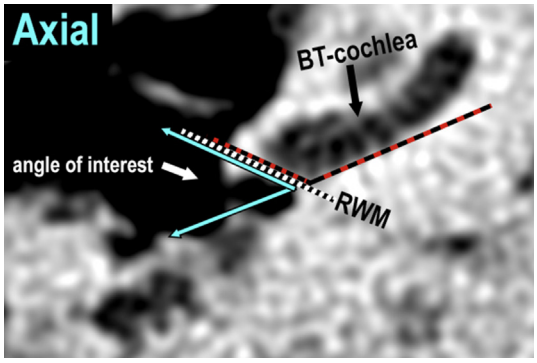

Figure 1 Angle of RWM relative to BT-Coch (∠RWBT). Reference angle is drawn along the BT-Coch at its intersection with the RWM. The angle of interest (dotted) is the supplementary angle, and the mean was found to be (42.1 ± 8.6)°.

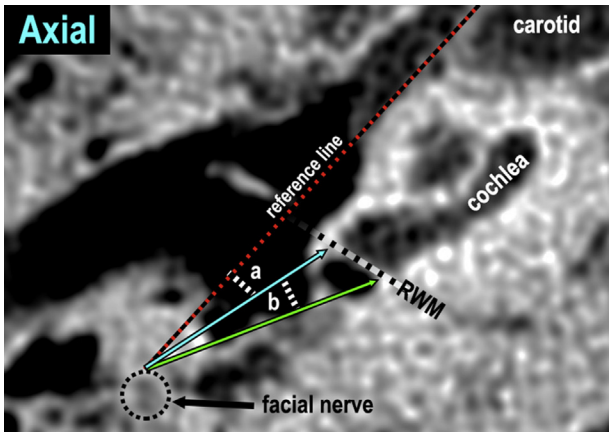

Figure 2 Measurements from AFN to demonstrate RWM position and visibility. Reference line is drawn from anterior edge of facial nerve to lateral wall of carotid canal. The black circle outlines the mastoid segment of the facial nerve. Angles are measured to medial and lateral edges of the RWM. Angle 'a' designates the degrees of adjustment (∠DOA) necessary to locate the RWN, which is located a mean (14.7 ± 5.2)° posterior from AFN-CA. Angle 'b' corresponds to the degrees of freedom (∠DOF), representing RWM visibility with a mean of (12.5 ± 2.6)°.

TA. In axial plane, coordinates were recorded at the window just inferior to umbo tip (Fig. 4). In coronal plane, coordinates were recorded in the same window as umbo tip (Fig. 5). Prominent landmarks were mid-RWM and TA. In order to generate a reference line, a tertiary point was marked at the most narrowed portion of external auditory canal (nEAC) in the same window as TA coordinate. Calculation was conducted on coordinates obtained from two separate slices because mid-RWM and TA cannot be visualized in a single plane. The line connecting TA and mid-RWM represented the vector of interest. A schematic flow

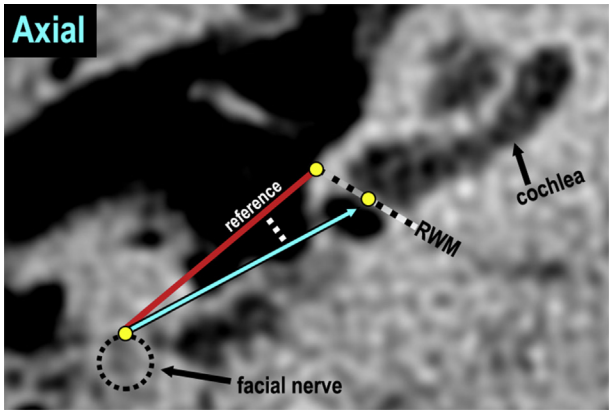

Figure 3 Distance and trajectory from AFN to mid-RWM. Coordinates (solid circles) are marked at AFN, RWN, and mid-RWM. AFN-RWN reference line is labeled as above. The vector (arrow) directed from AFN to the mid-RWM measured (6.2 ± 0.8) mm in mean length, and was oriented an average (8.6 ± 3.9)° posteriorly from the reference line.

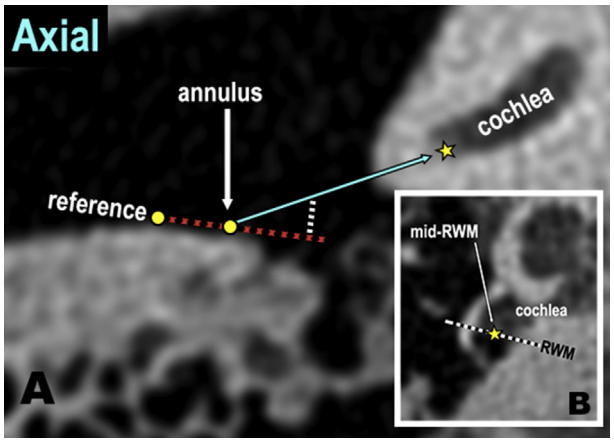

Figure 4 Axial plane determination of TA-RWM distance and trajectory. Coordinates were obtained at EAC and posterior TA (solid circles), and mid-RWM (star). The star marks the position of the mid-RWM seen on another slice (inset image) to better illustrate its location despite not being anatomically aligned with the annulus in axial and coronal planes. EAC-TA reference line is shown above. TA is (5.4 ± 0.8) mm on average from the mid-RWM. The dashed white line in main image labels the angle of the calculated vector relative to EAC-TA reference line, and measures on average (19.1 ± 11.1)°.

diagram available online detailed how these coordinates were obtained on OsiriX (Supplement 2).

Distance and trajectory from umbo to mid-RWM

For both axial and coronal planes, the umbo tip was used as it represents a visible bony landmark from EAC. A reference line was drawn from umbo tip to inferior TA (coronal) and posterior TA (axial). Measurements were obtained from multiple slices, as umbo tip and mid-RWM were not visible in the same slice. Coordinates were recorded for umbo tip and mid-RWM — the line connecting these points represented the vector of interest.

Using angle and length measurements of the above vector, x- and y-coordinates were obtained using trigonometric functions — cosine for x-coordinates and sine for y-coordinates. These points were individually graphed and subsequently overlaid on an image of the TM to demonstrate variability in mid-RWM location with umbo tip serving as the origin on coordinate plane (Fig. 6).

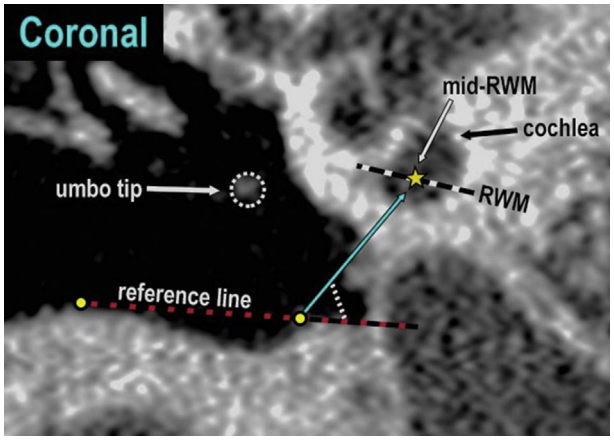

Figure 5 Coronal plane determination of TA-RWM distance and trajectory. Coordinates were obtained at EAC and inferior TA (solid circles), and mid-RWM (star). The star marks the position of the mid-RWM. EAC-TA reference line is shown above. TA is (4.1 ± 1.4) mm mean length from mid-RWM. The dashed white line denotes the vector angle relative to EAC-TA reference line, and measures a mean of (77.1 ± 27.9)°.

Results

In the final sample of 100 studies, 55% were female. The mean age was 49.2 years (range 19—72 years; standard deviation 17.7 years). The most common indication for imaging was hearing loss; others included tinnitus, pain, and aural fullness. All studies were read as normal by experienced neuroradiologists.

Table 1 shows summary statistics for all measurements defined by this study.

Measurements relevant to CI

1. The mean RWM angle relative to BT-Coch (∠RWBT) was (42.1 ± 8.6)°. Four of 100 total ears were outside two standard deviations (2SD) (Fig. 1). This angle demonstrated that the RWM is tilted posteriorly, and more acute ∠RWBT may make direct RWI difficult.

2. Mean RWM visibility from FR measured by degrees of freedom (∠DOF) was (12.5 ± 2.4)°. Five total ears were outside 2SD. Serving as proxy for RWM position, the mean (∠DOA) was (14.7 ± 5.2)°. Only 1 ear was found outside 2SD (Fig. 2). These measurements indicated the RWM is slightly posteriorly situated from the plane of the FN as seen through the FR. Significantly increased posterior rotation of RWM may have surgical implications for access to RWM during CI insertion.

3. Mean Vector length from AFN to mid-RWM was (6.2 ± 0.8) mm. Six ears were outside 2SD based on vector length. Longer vector length in combination with more

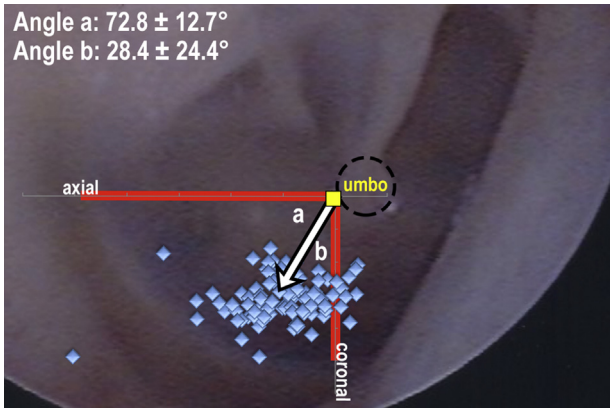

Figure 6 Otoscopic image from external auditory canal. The scatterplot represents the variation seen in the location of the RWM midpoint. The arrow represents the distance and trajectory from umbo to the average of these points.

Table 1 Summary statistics for measurements.

Measurement	Plane	Type of measure (Unit)	Mean	Standard deviation
RWM at junction with basal turn posterior bony boundary (∠RWBT)	Axial	Angle (°)	42.1	8.6
RWM visibility from facial recess (Degrees of freedom, ∠DOF)	Axial	Angle (°)	12.5	2.4
RWM position from facial recess (Degrees of adjustment, ∠DOA)	Axial	Angle (°)	14.7	5.2
Vector — AFN to mid-RWM	Axial	Length (mm)	6.2	0.8
		Angle (°)	8.6	3.9
Vector — TA to mid-RWM	Axial	Length (mm)	5.4	0.8
		Angle (°)	19.1	11.1
Vector — TA to mid-RWM	Coronal	Length (mm)	4.1	1.4
		Angle (°)	77.1	27.9
Vector — umbo to mid-RWM	Axial	Length (mm)	3.3	0.7
		Angle (°)	72.8	12.7
Vector — umbo to mid-RWM	Coronal	Length (mm)	4.5	0.8
		Angle (°)	28.4	24.4

RWM: round window membrane; AFN: anterior edge of facial nerve; TA: tympanic annulus.

posterior RWM trajectory may necessitate transcanal exposure of the RWM in certain cases. The RWM trajectory was shifted posteriorly an average of (8.6 ± 3.9)° from AFN-RWM reference line, with 4 ears outside 2SD (Fig. 3).

Measurements relevant to TDD

1. Mean vector length from posterior TA to mid-RWM was (5.4 ± 0.8) mm (3 ears outside 2SD), and was oriented an average (19.1 ± 11.1)° (4 ears outside 2SD) anteriorly from the reference line along posterior TA on axial view (Fig. 4). On coronal reformat, the mean length of the vector from inferior TA to mid-RWM was (4.1 ± 1.4) mm, and average trajectory was oriented (77.1 ± 27.9)° superior from reference line drawn through inferior TA. Nine ears were outside 2SD for both length and trajectory (Fig. 5).

2. Mean Vector length from umbo to mid-RWM in axial plane was (3.3 ± 0.7) mm (three ears outside 2SD), and was on average oriented (72.8 ± 12.7)° (four ears outside 2SD) (angle a in Fig. 6) anteroinferiorly from umbo-posterior TA reference line and medial to umbo tip, which served as the main reference point. In coronal plane, the mean length was (4.5 ± 0.8) mm (one ear outside 2SD) and oriented an average (28.4 ± 24.4)° (four ears outside 2SD) (angle b in Fig. 6) posteroinferiorly from umbo-inferior TA reference line and medial to the umbo tip. Fig. 6 illustrates this variability in RWM location relative to the umbo. Thus, the mean distance of RWM from the umbo was 4 mm along the vector posteriorly rotated approximately 30° clockwise from a perpendicular drawn from umbo to inferior TA. Together, these measurements placed RWM position predominantly in the middle of the posteroinferior quadrant.

Discussion

Cochlear implantation

Considerable debate remains on ideal electrode insertion method, with data supporting all approaches or showing no substantial difference.[3,14,15] However, RWI facilitated more proper placement in the scala tympani and caused less basal cochlear damage.[3,16–18] For these considerations, patients may benefit from RWI if anatomy permits.

A thick bony overhang may obscure RWM position and orientation. Park and colleagues measured the overhang thickness on four consecutive axial slices, and found no correlation with intraoperative difficulty of accessing the RW.[19] However, this bony overhang is often drilled away for adequate RWM visualization. This lack of association reflects this, and may suggest RWM orientation is more representative of predicting surgical difficulty.

This study defines RWM orientation as ∠RWBT, which was a mean (42.1 ± 8.6)°, which reflects the non-uniform configuration suggested by Atturo et al.[20] As ∠RWBT decreases, the RWM directs more posteriorly and becomes challenging to access from FR because less surface is visible. Previously, an anatomical study demonstrated that insertional trauma was less likely from FR approach if RWM visibility was greater.[21] We believe understanding this angle may allow surgeons to modify trajectory or widen the FR for proper electrode insertion to minimize intracochlear damage from electrode contact with the lateral cochlear wall and modiolus.

Kashio et al[22] defined the EAC angle in a retrospective case series to predict surgical visualization of RWM during surgery. This angle — formed by lines through the EAC bony-cartilaginous junction and through the center of the BT-Coch — positively correlated with RWN visibility. This is useful because location of the EAC can limit visualization of RWM through the FR and may need to be thinned to fully expose RWM for safer electrode insertion.

Even small variation in RWM visibility may significantly affect surgical access. Very limited RWM visibility through FR may necessitate thinning the posterior ear canal wall during CI, extending the bony RW, or even transcanal exposure for particularly difficult cases.[23] Although this is an intraoperative determination, predicting need for these maneuvers is possible preoperatively - understanding normal range of RWM visibility may alert the surgeon to specific obstacles that may necessitate these maneuvers thereby allowing appropriate counseling.

CI insertion vectors have been evaluated previously by Meshik and colleagues, who examined the intracochlear structures of 8 cadaveric TBs using micro-CT.[4] Using custom programming software, these authors identified one vector passing through mid-RWM and remaining tangent to the scala tympani centerline. However, they suggested such an insertion vector necessitated too extreme flexibility for standard cochlear implant electrode arrays.

OsiriX coordinates are a novel way to identify electrode insertion vectors. These dictate whether you might need to modify your approach — for example, shorter or posterior-angulated vectors reflect more difficult anatomy. Our data shows vector distance is reliable among the sample, but trajectory is more variable. This may reflect the difficulty in pinpointing the RWM midpoint in two-dimensional space given its nonplanar ovoid shape.[20] If degree of posterior angulation is unfavorable, it is important to maximize the FR exposure by thinning the ear canal, completely removing bone anterior to the FN, or even sacrificing the chorda tympani. Modifications such as retrofacial approach or transcanal-assisted cochleostomy should be considered in extreme cases.[24–26]

Although TBCTs are conventionally obtained using multidetector CT, new strategies continue to develop as otologic surgeons strive to improve CI and its outcomes. CBCT is an evolving technology that permits cross-sectional imaging of distinct areas using lower radiation doses, and has been reported in multiple cadaveric studies to be of comparable image quality when used intraoperatively.[27–31] Anatomy segmentation on preoperative CT scans has also been proposed as a means to algorithmically define an electrode insertion vector and allow for image guidance.[32–34] While the study authors believe these are promising endeavors in CI research, we do not have the availability and experience with these technologies at our institution. An intraoperative means of optimizing electrode insertion is ideal — however, the current data is limited by the paucity of clinical data on human models and by lack of widespread applicability due to limited availability of equipment. We hope the measurements described in this study will benefit otologic surgeons who perform CI at institutions that rely on standard multidetector CT images.

Transtympanic drug delivery

Direct application for diffusion across the RWM helps both to minimize systemic side effects and bolster therapeutic concentration locally.[35,36] TDD may modestly improve symptoms after failed systemic treatments, or even achieve higher inner ear drug concentrations with combination therapy.[37,38] The TA and umbo are important bony landmarks visible during ear microscopy and are useful references in TDD. By understanding their relationships to the RWM, practitioners can achieve improved therapeutic delivery to the inner ear.

RW anatomic variation is especially important to recognize in TDD as precise injection near RWM is necessary for optimal therapeutic delivery — this is to select optimal injection sites maximize drug perfusion across the RWM. Our CT-based measurements indicate that RWM was located an average of 4 mm away from the umbo along the 5-and 7-o'clock radial vector for the left and right ear, respectively. Therefore, TDD injections should be in the posteroinferior quadrant of the TM within 4 mm of the umbo. Knowing the RWM location using external bony landmarks increases the likelihood that injected drug contacts the maximum area of RWM, optimizing permeation into the inner ear. This may become even more important as the field moves toward therapeutic delivery via long-acting or sustained release vehicles.[3]

This study faces some limitations. Because coordinates were acquired on multiple slices, calculations of vector distance and trajectory from FN, umbo, and TA to the mid-RWM may be imprecise. Further complicating acquisition of these coordinates is the nonplanar "saddle like" conformation of the RWM.[20] Axial sections incompletely reflect RWM in true three-dimensional view as afforded by surgery — this is the experience of the neurotologists who perform these procedures at our institution. However, the authors identified these measurements to provide an approximation of RWM position for surgical planning to supplement preoperative and intraoperative decision-making.

Linear measurements on multiplanar reconstruction (MPR) were reported to vary between imaging planes and may underestimate or overestimate actual physical size.[39,40] This may explain differences in vector properties between axial and coronal images seen in this study. Despite this, MPR produces comparable images to direct axial and coronal scanning.[41] The accuracy of linear measurements on CT imaging to live patient anatomy is difficult to validate and protocols are difficult to standardize, as many previously studies vary greatly in their methodology and hardware.[42] Furthermore, reliability of these measurements highly depends on image quality and on clarity of defining the landmark.[43]

Conclusion

TBCTs are common imaging modalities for otologic evaluation, providing opportunities to preoperatively assess RW anatomy. The radiologic measurements defined in this study demonstrate normal RW anatomic variations relative to the FR and transtympanic approaches. ∠RWBT reflects orientation of the RWM, while ∠DOA and ∠DOF represent RWM position and visibility relative to FR — these may aid in determining favorability of RWI. Those relevant to TDD aim to enhance our understanding of RWM localization relative to externally visible TM landmarks. Vector lengths are reliable among the sample, but trajectory typically deviates from the average. The RWM was located on average 4 mm away from umbo tip, and TDD should be injected within 4 mm of umbo tip into the TM's posteroinferior quadrant.

Financial support and funding

None.

Financial disclosures

The authors have no financial disclosure.

Declaration of Competing Interest

The authors report no conflicts of interest.

Appendix A. Supplementary data

Supplementary data to this article can be found online at https://doi.org/10.1016/j.wjorl.2018.12.003.

References

1. Aslan A, Tekdemir I, Gunhan K, Eskiizmir G, Elhan A. Anatomic observations on variations of the round window niche and its relationship to the tympanic membrane. *Mediterr J Otol*. 2006; 2:52—57.
2. Richard C, Fayad JN, Doherty J, Linthicum Jr FH. Round window versus cochleostomy technique in cochlear implantation: histologic findings. *Otol Neurotol*. 2012;33:1181—1187.
3. Wanna GB, Noble JH, Carlson ML, et al. Impact of electrode design and surgical approach on scalar location and cochlear implant outcomes. *Laryngoscope*. 2014;124(suppl 6):S1—S7.
4. Meshik X, Holden TA, Chole RA, Hullar TE. Optimal cochlear implant insertion vectors. *Otol Neurotol*. 2009;31:58—63.
5. Tamplen M, Schwalje A, Lustig L, Alemi AS, Miller ME. Utility of preoperative computed tomography and magnetic resonance imaging in adult and pediatric cochlear implant candidates. *Laryngoscope*. 2016;126:1440—1445.
6. McRackan TR, Reda FA, Rivas A, et al. Comparison of cochlear implant relevant anatomy in children versus adults. *Otol Neurotol*. 2012;33:328—334.
7. Lloyd SK, Kasbekar AV, Kenway B, et al. Developmental changes in cochlear orientation — implications for cochlear implantation. *Otol Neurotol*. 2010;31:902—907.
8. Formeister EJ, Campbell AP, Choudhury B, Huang B, Jewells V, Adunka OF. The relationship between cochleovestibular orientation, age and sensorineural hearing loss: implications for cochlear implantation. *Ann Otol Rhinol Laryngol*. 2015;124: 681—690.
9. Swan EE, Mescher MJ, Sewell WF, Tao SL, Borenstein JT. Inner ear drug delivery for auditory applications. *Adv Drug Deliv Rev*. 2008;60:1583—1599.
10. Robey AB, Morrow T, Moore GF. Systemic side effects of transtympanic steroids. *Laryngoscope*. 2010;120(suppl 4):S217.
11. Kim G, Jung HJ, Lee HJ, Lee JS, Koo S, Chang SH. Accuracy and reliability of length measurements on three-dimensional computed tomography using open-source OsiriX software. *J Digit Imaging*. 2012;25:486—491.
12. Yamauchi T, Yamazaki M, Okawa A, et al. Efficacy and reliability of highly functional open source DICOM software (OsiriX) in spine surgery. *J Clin Neurosci*. 2010;17:756—759.
13. Deshpande AS, Wendell Todd N. Implanting straight into cochlea risks the facial nerve: a Cartesian coordinate study. *Surg Radiol Anat*. 2016;38:1153—1159.
14. Sun CH, Hsu CJ, Chen PR, Wu HP. Residual hearing preservation after cochlear implantation via round window or cochleostomy approach. *Laryngoscope*. 2015;125:1715—1719.
15. Zhou L, Friedmann DR, Treaba C, Peng R, Roland Jr JT. Does cochleostomy location influence electrode trajectory and intracochlear trauma? *Laryngoscope*. 2015;125:966—971.
16. Connor SE, Holland NJ, Agger A, et al. Round window insertion potentiates retention in the scala tympani. *Acta Otolaryngol*. 2012;132:932—937.
17. Atturo F, Barbara M, Rask-Andersen H. On the anatomy of the 'hook' region of the human cochlea and how it relates to cochlear implantation. *Audiol Neurotol*. 2014;19:378—385.
18. Adunka O, Unkelbach MH, Mack M, Hambek M, Gstoettner W, Kiefer J. Cochlear implantation via the round window membrane minimizes trauma to cochlear structures: a histologically controlled insertion study. *Acta Otolaryngol*. 2004;124: 807—812.
19. Park E, Amoodi H, Kuthubutheen J, Chen JM, Nedzelski JM, Lin VY. Predictors of round window accessibility for adult cochlear implantation based on pre-operative CT scan: a prospective observational study. *J Otolaryngol Head Neck Surg*. 2015;44:20.
20. Atturo F, Barbara M, Rask-Andersen H. Is the human round window really round? An anatomic study with surgical implications. *Otol Neurotol*. 2014;35:1354—1360.
21. Shapira Y, Esraghi AA, Balkany TJ. The perceived angle of the round window affects electrode insertion trauma in round window insertion — an anatomical study. *Acta Otolaryngol*. 2011;131:284—289.
22. Kashio A, Sakamoto T, Karino S, Kakigi A, Iwasaki S, Yamasoba T. Predicting round window niche visibility via the facial recess using high-resolution computed tomography. *Otol Neurotol*. 2015;36:e18—e23.
23. Leong AC, Jiang D, Agger A, Fitzgerald-O'Connor A. Evaluation of round window accessibility to cochlear implant insertion. *Eur Arch Otorhinolaryngol*. 2013;270:1237—1242.
24. Kiumehr S, Mahboubi H, Middlebrooks JC, Djalilian HR. Transcanal approach for implantation of a cochlear nerve electrode array. *Laryngoscope*. 2013;123:1261—1265.
25. Allen KP, Bartels LJ, Isaacson B. Cochlear implantation requiring a retrofacial approach to the round window. *Otol Neurotol*. 2015;36:e84—e86.
26. Rizk H, O'Connell B, Stevens S, Meyer T. Retrofacial approach to access the round window for cochlear implantation of malformed ears. *Otol Neurotol*. 2015;36:e79—e83.
27. Erovic BM, Chan HH, Daly MJ, et al. Intraoperative cone-beam computed tomography and multi-slice computed tomography in temporal bone imaging for surgical treatment. *Otolaryngol Head Neck Surg*. 2014;150:107—114.
28. Barker E, Trimble K, Chan H, et al. Intraoperative use of cone-beam computed tomography in a cadaveric ossified cochlea model. *Otolaryngol Head Neck Surg*. 2009;140:697—702.
29. Rafferty M, Siewerdsen JH, Chan Y, et al. Intraoperative cone-beam CT for guidance of temporal bone surgery. *Otolaryngol Head Neck Surg*. 2006;134:801—808.
30. Cushing SL, Daly MJ, Treaba CG, et al. High-resolution cone-beam computed tomography: a potential tool to improve atraumatic electrode design and position. *Acta Otolaryngol*. 2012;132:361—368.
31. Zou J, Lahelma J, Koivisto J, et al. Imaging cochlear implantation with round window insertion in human temporal bones and cochlear morphological variation using high-resolution cone beam CT. *Acta Otolaryngol*. 2015;135:466—472.
32. Reda FA, McRackan TR, Labadie RF, Dawant BM, Noble JH. Automatic segmentation of intra-cochlear anatomy in post-implantation CT of unilateral cochlear implant recipients. *Med Image Anal*. 2014;18:605—615.
33. Labadie RF, Balachandran R, Noble JH, et al. Minimally invasive image-guided cochlear implantation surgery: first report of clinical implementation. *Laryngoscope*. 2014;124:1915—1922.
34. Labadie RF, Noble JH. Preliminary results with image-guided cochlear implant insertion techniques. *Otol Neurotol*. 2018; 39:922—928.
35. Lustig LR. The history of intratympanic drug therapy in otology. *Otolaryngol Clin North Am*. 2004;37:1001—1017.
36. Miller MW, Agrawal Y. Intratympanic therapies for Menière's disease. *Curr Otorhinolaryngol Rep*. 2014;2:137—143.
37. Haynes DS, O'Malley M, Cohen S, Watford K, Labadie RF. Intratympanic dexamethasone for sudden sensorineural hearing loss after failure of systemic therapy. *Laryngoscope*. 2007; 117:3—15.

38. Kanzaki S, Fujioka M, Yasuda A, et al. Novel in vivo imaging analysis of an inner ear drug delivery system in mice: comparison of inner ear drug concentrations over time after transtympanic and systemic injections. *PLoS One*. 2012;7, e48480.
39. Lisanti CJ, Oettel DJ, Reiter MJ, Schwope RB. Multiplanar reformations in the measurement of renal length on CT: is it plain which plane to use? *AJR Am J Roentgenol*. 2015;205: 797—801.
40. Ridge CA, Huang J, Cardoza S, et al. Comparison of multiplanar reformatted CT lung tumor measurements to axial tumor measurement alone: impact on maximal tumor dimension and T stage. *AJR Am J Roentgenol*. 2013;201:959—963.
41. Venema HW, Phoa SS, Mirck PG, Hulsmans FJ, Majoie CB, Verbeeten Jr B. Petrosal bone: coronal reconstructions from axial spiral CT data obtained with 0.5-mm collimation can replace direct coronal sequential scans. *Radiology*. 1999;213: 375—382.
42. Vasconcellos ACRS, da Silva Maciel A, Rubira CMF, Rubira-Bullen IRF, Sarmento VA. Accuracy of linear measurement in computed tomography: a systematic review. *Int J Enhanced Res Sci Technol Eng*. 2015;4:79—88.
43. Lou L, Lagravere MO, Compton S, Major PW, Flores-Mir C. Accuracy of measurements and reliability of landmark identification with computed tomography (CT) techniques in the maxillofacial area: a systematic review. *Oral Surg Oral Med Oral Pathol Oral Radiol Endod*. 2007;104:402—411.

Edited by Xin Jin